Microscopic origin of gray tracks in $KTiOPO_4$

A. Bocchini,* U. Gerstmann, and W. G. Schmidt
Department Physik, Universität Paderborn, Paderborn 33095, Germany

(Received 4 November 2024; revised 10 February 2025; accepted 21 February 2025; published 7 March 2025)

In this paper, O-vacancy-related Ti^{3+} centers in potassium titanyl phosphate ($KTiOPO_4$, KTP), which are commonly discussed along the formation of its characteristic photochromic damage (i.e., so-called gray tracking), are systematically investigated within density functional theory. Notably, centers localized at TiO_6 moieties close the vacancy, provide the best agreement with experimental hyperfine tensors, and are also energetically more favorable compared to the ones located at undercoordinated TiO_5 moieties, whereby displaced K ions are found to stabilize them. Ti^{3+} centers embedded in Rb-doped KTP share the same properties as those in stoichiometric KTP. The calculated absorption spectra for K-deficient KTP suggest that gray tracking can be attributed to a vacancy pair composed of a positively charged O vacancy and a negatively charged K vacancy. The displaced K ions could contribute to the local formation of overpopulated K channels, which may also be associated with gray tracking.

DOI: 10.1103/PhysRevB.111.104103

I. INTRODUCTION

Potassium titanyl phosphate ($KTiOPO_4$, KTP) is arguably the best-known member of the ferroelectric crystal family, with the general constitution formula $MTiOXO_4$. Its peculiar crystal structure, see Fig. 1 (details can be found in, e.g., Refs. [1–4]), determines a number of interesting properties, allowing for its application in many different fields. To name some examples, KTP crystals are already well established as frequency doublers, waveguides, or electro-optic modulators, and have recently been proposed as a possible electrode material [4–17]. Unfortunately, the usage of KTP is limited by the possibility of characteristic photochromic damage (i.e., so-called gray tracks or gray tracking), showing absorption characteristics for application-relevant wavelengths (i.e., 1064 nm and 532 nm), whereby the operation of damaged crystals can lead to their catastrophic failure [1,18–29].

The macroscopic formation of gray tracks has been reported during a variety of processes, e.g., upon the application of strong electric fields [25,26], the irradiation with high-intensity laser light [17–20] or x-rays [27], or even the reduction at high temperatures in H_2 atmospheres [28].

The microscopic origin of gray tracks, on the other hand, is commonly attributed to the formation of Ti^{3+} centers (i.e., reduced titanium atoms) as the result of the charge compensation of O vacancies, which naturally form upon charge compensation for K vacancies [1,20,22,23,30–35]. In KTP, there are two types of O, which differ with respect to their coordination: Eight atoms [O(1)–O(8)] are coordinated to P and Ti, while sites O(9) and O(10) bond to Ti exclusively (see also Fig. 1). Only the latter type is relevant for gray tracking [1,31,34–37]. More precisely, the only thermally stable Ti^{3+} center (A_{flx} [23,34]) has been attributed to a reduced Ti(2) atom adjacent to a single positively charged O(10) vacancy by experiment [34] and theory [35]. In addition, a recent density functional theory (DFT) study [38] reported that different stages of gray tracking could be explained by different charge states assumed by the O(10) vacancy itself.

Besides, when it comes to their suppression, treatments leading to (i) a reduced number of potassium vacancies [1,26] or (ii) a reduced mobility of K ions along [001] via, e.g., Rb dopants [1,39], were found to be very efficient. Notably, the properties of oxygen vacancies in K-deficient KTP and their possible role during gray tracking are still not completely understood [40]. Also, Rb seems to play a rather controversial role in this context: While moderate Rb doping is helpful to increase the threshold against gray tracking [1,26,39], the same O-vacancy-related Ti^{3+} center has been detected in $RbTiOPO_4$ (RTP) crystals [41], which indeed assume a grayish coloring [41], but are less affected by gray tracking [39]. In addition, both KTP and RTP are reported to show similar laser-damage behaviors [42].

Moreover, also the exact localization of the O-vacancy-related Ti^{3+} centers might be controversial, similar to the case of titania, where a number of different configurations were found, in which the position of O-vacancy-related Ti^{3+} centers is not limited to Ti atoms directly adjacent to the vacancy itself (i.e., the ones in undercoordinated TiO_5 mojeties) [43].

Clearly, all these open questions indicate that the attribution of gray tracks to oxygen vacancies alone may provide an oversimplified picture for such a complex phenomenon. In the following, we aim at exploring the electronic [40] and magnetic [40], as well as optical properties of O vacancies and related Ti^{3+} centers within application-relevant chemical environments, i.e., in Rb-doped as well as K-deficient KTP crystals. In addition, we investigate the effects arising from the relative position of the Ti^{3+} and the O vacancy within the lattice. More precisely, we localize them both at undercoordinated Ti(2)O_5 polyhedra caused by the O vacancy itself and

*Contact author: adriana.bocchini@upb.de

 ©2025 American Physical Society

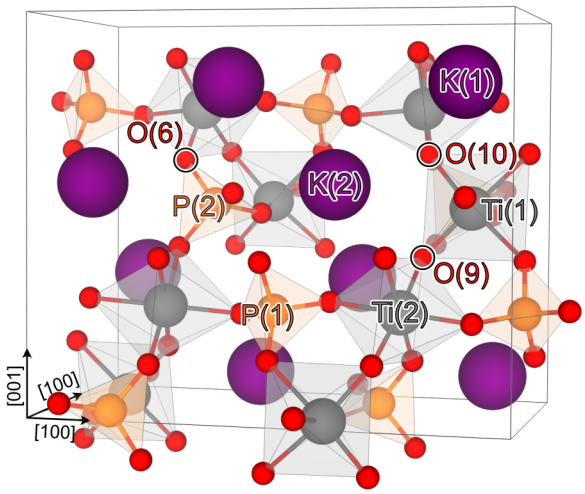

FIG. 1. Schematic representation (All the here shown crystal structures as well as charge densities were visualized using the VESTA [44] program.) of the KTP unit cell. Ti, P, K, and O atoms are depicted in gray, orange, purple, and red, respectively. The position of relevant lattice sites is indicated. Two O types can be identified in the cell: The atoms O(1)–O(8) [site O(6) is marked] are coordinated to both Ti and P, the atoms O(9) and O(10), on the other hand, to Ti exclusively.

at $Ti(2)O_6$ moieties close to the vacancy. Thus, we contribute to a better understanding of the gray-track formation in KTP.

II. COMPUTATIONAL

Calculations are performed using DFT as implemented in the open-source package QUANTUM ESPRESSO [45,46]. For the fully relaxed defect structures, optical properties are computed using the YAMBO code [47,48].

Oxygen vacancies (V_O) are embedded in stoichiometric KTP using a 64-atom supercell (i.e., eight repetitions of the formula unit $KTiOPO_4$), as well as in K-deficient KTP and a rubidium-doped KTP supercell, both highly relevant for the gray-tacking mechanism [1,26,39]. The defect structures are fully relaxed using the Baldereschi point [49] for Brillouin zone sampling. For the optical properties, on the other hand, a finer mesh of $3 \times 6 \times 3\,\boldsymbol{k}$ points is used.

During the calculations, the lattice constants are kept fixed at their experimental values [50] of $a = 12.814$ Å, $b = 6.404$ Å, and $c = 10.616$ Å, while the atomic positions are optimized until fluctuations of the total energy and forces are lower than the thresholds of 10^{-8} Ry and 10^{-4} Ry/bohr, respectively. Details of the resulting defect geometries can be found in Sec. III.

At the lowest level of theory, the electronic exchange and correlation effects are described within the generalized gradient approximation, more precisely via the PBEsol [51,52] functional. We apply norm-conserving pseudopotentials treating the Ti $3d^2\,3s^2\,3p^6$, P $3s^2\,3p^3$, K $4s^1$, Rb$5s^1$, and O $2s^2\,2p^4$ states as valence states. These yield an electronic band gap of $E_{\rm gap}^{\rm PBEsol} = 3.27$ eV, slightly larger compared to the ones reported in our previous studies [35,37,38]. This is related to the use of a Ti pseudopotential with a larger number of valence states (semicore $3s\,3p$ states in the valence). As reported by Neufeld *et al.* [53] in fact, the magnitude of the KTP band gap tends to be enlarged in this case.

To improve the description of the reduction of Ti atoms (i.e., the formation of Ti^{3+} centers), we apply the Hubbard correction [54] (PBEsol + U) on the Ti $3d$ states. The application of this correction is reasonable, since it is well-known to yield an accurate description of the localization of the $3d$ wave functions and by this improved hyperfine tensors of Ti^{3+} centers in KTP [35]. The Hubbard U is included via the simplified scheme by Cococcioni and de Gironcoli, and the magnitude of the correction is self-consistently determined using the methodology discussed in Ref. [54]. This procedure yields the values of $U_1 = 5.91$ eV and $U_2 = 5.87$ eV for the two different Ti sites Ti(1) and Ti(2), respectively. We note that the self-consistently determined U parameters for the Ti $3d$ electrons in cells containing Rb dopants, K vacancies, and/or reduced Ti^{3+} centers do not deviate more than 0.15 eV from the ones in the stoichiometric bulk KTP cell. Thus, for the sake of simplicity, we adopt an average value of $U = 5.9$ eV for all Ti atoms in all simulations.

With the Hubbard correction, the band gap widens to $E_{\rm gap}^{+U} = 3.61$ eV. This value perfectly fits in the range of band-gap widths reported for KTP, i.e., $E_{\rm gap}^{\rm exp} = 3.2$-$3.8$ eV [7,55–57]. Thus, the Ti pseudopotential used here enables us to correctly describe the KTP band gap already at the PBEsol + U level of theory. Nevertheless, since the energetic position of the defect level in the gap critically depends on the exact U value, we use the standard PBE0 [58] hybrid functional to confirm the relative stability of the defects and to determine the energetic position of the O-vacancy related midgap states [59–61].

To determine which defects prevail for a given Fermi-level position (ε_F), we compute their formation energy $E_{\rm form}$ defined as

$$E_{\rm form} = E_{\rm def} - E_{\rm ideal} - \sum_i n_i \mu_i + q \cdot \varepsilon_F . \qquad (1)$$

Here, $E_{\rm def}$ refers to the ground-state energy of the supercell containing the defects, $E_{\rm ideal}$ to the energy of the ideal supercell (here stoichiometric, K-deficient, or Rb-doped KTP), $n_i < 0$ is the number of atoms removed ($n_i > 0$ if added) from (to) the supercell, μ_i the chemical potential of the respective elements, and q denotes the defect's charge state. In this paper, we determine the formation energy of O vacancies as well as K vacancies and K interstitials. The related chemical potentials are determined using molecular oxygen and metallic potassium. For the determination of the charge-transition states ($N/N+1$), we apply the so-called Slater-Janak model, allowing for their direct computation via

$$(N/N+1) = E^{N+1} - E^N = \varepsilon_H\left(\frac{1}{2}\right), \qquad (2)$$

with E^{N+1} and E^N as the energies of a supercell containing $N+1$ and N electrons, respectively, and $\varepsilon_H(\frac{1}{2})$ as the one-particle energy of the highest Kohn-Sham orbital affected by the charge transition with an occupation of $1/2$ with respect

to the valence band maximum (VBM) of the ideal supercell (here, stoichiometric, K-deficient, or Rb-doped KTP) [62–64].

To identify the most likely defect structure, experimentally observed hyperfine (hf) splittings are compared with hf parameters theoretically determined for selected defect models. They are calculated in scalar-relativistic approximation using the gauge-including projector augmented plane wave approach (GIPAW) [65] as implemented in the QUANTUM ESPRESSO package [45,46] and require an analysis of the magnetization density $m(\vec{r}) = n^{\uparrow}(\vec{r}) - n^{\downarrow}(\vec{r})$ (i.e., the probability of the unpaired electrons) in a small region around the nuclei [66].

Assuming efficient orbital quenching by the crystal ligand field [67], the hyperfine interaction due to a nucleus I at the position $\vec{r}_I$ can be split into two contributions: (i) the isotropic Fermi contact term

$$a_I = \frac{1}{2S}\frac{8\pi}{3}\gamma_I \int m(\vec{r})\,\delta_{\mathrm{Th}}(\vec{r}-\vec{r}_I)\,d^3\vec{r}, \tag{3}$$

where $\gamma_I = 2g_N^k\,\mu_B\,\mu_N\frac{\mu_0}{4\pi}$ and $\delta_{\mathrm{Th}}(\vec{r}-\vec{r}_I)$ represents a broadened δ function with half width given by the Thomas radius $r_{\mathrm{Th}} = \frac{Ze^2}{mc^2}$, about 10 times the nuclear radius, and (ii) a purely anisotropic term due to the dipole-dipole interaction of the electronic magnetization density $m(\vec{r})$:

$$\underline{\underline{B}}_I = \frac{1}{2S}\gamma_I \int m(\vec{r})\frac{3(\vec{r}-\vec{r}_I)\otimes(\vec{r}-\vec{r}_I) - |\vec{r}-\vec{r}_I|^2\underline{\underline{1}}}{|\vec{r}-\vec{r}_I|^5}d^3\vec{r}. \tag{4}$$

Diagonalization of the resulting hf tensor $\underline{\underline{A}}_I = a_I\underline{\underline{1}} + \underline{\underline{B}}_I$ yields the principal hyperfine values A_i listed in Table I.

For the most likely defect structures, we calculate the optical absorption following the approach discussed in Ref. [38], e.g., we apply the independent particle approximation using the electronic structure as calculated via a modified PBE0 functional including a reduced fraction α of exact exchange (EXX) from Hartree-Fock theory (i.e., PBE0-α), which was shown to yield [38] optical properties in close agreement with the established GW + BSE quasiparticle formalism [53,68].

III. STRUCTURAL DETAILS

In a previous DFT study [35], the best agreement with the experimental hyperfine tensors [34] of the thermally stable Ti^{3+} center was found for the one caused by a O(10) vacancy leading to the reduction of the adjacent Ti(2) atom. A quantitative analysis of the two datasets, however, points out some deviation from experiment: The DFT values for the nucleus ^{31}P(1) are slightly overestimated, while the ones for ^{31}P(2) and ^{31}P(3) are clearly smaller than the corresponding experimental values, cf. Refs. [34,35].

To investigate the influence of the local chemical environment of the Ti^{3+} centers, the O vacancy is inserted in different host materials, i.e., in stoichiometric KTP, K-deficient as well as Rb-doped KTP, whereby all chemical environments are relevant in the context of gray tracking [1,26,39]. Due to the high mobility of the K ions along the [001] crystal direction, K-deficient KTP is modeled by placing potassium vacancies on either the K(1) or the K(2) lattice site. In addition, since the neutral charge state is expected to be energetically unstable [37] (also see Fig. 5), we model single negatively charged vacancies, i.e., $V^{-1}_{\mathrm{K(1)}}$ and $V^{-1}_{\mathrm{K(2)}}$. For Rb-doped KTP, on the other hand, because of the larger atomic radius of the Rb substitutionals and since they are more prone to occupy the larger K(2) cage [69], we only substitute a K(2) site by Rb. The relaxed unit cells of the four host materials are depicted in Fig. 2. Notably, the cell geometry is barely altered by the introduction of a Rb_K as well as a $V^{-1}_{\mathrm{K(1)}}$, while the vacancy $V^{-1}_{\mathrm{K(2)}}$ causes a local disorder in the K sublattice. In the following, we refer to Rb-doped cells as RKTP, while (depending on the position of the K vacancy) K-deficient cells are denoted as KTP-K1 and KTP-K2, respectively. Conceptionally, all four materials are treated as bulk (host) materials, whereby both KTP-K1, and KTP-K2 are single negatively charged, while ideal KTP and and the RKTP host material provide neutral supercells.

To model O-vacancy-related Ti^{3+} centers, O(9) as well as O(10) vacancies (both located between two Ti atoms, see Fig. 1) are introduced in these four host materials. Thereby, we focus on the electron-paramagnetic-resonant-active (EPR active) +1 charge states, which provide an unpaired electron yielding an $S = 1/2$ paramagnetic defect state.

To model Ti^{3+} centers located in undercoordinated TiO_5 and stoichiometric TiO_6 moieties, we adopt a two-step procedure to selectively reduce specific Ti atoms: First, the geometry of the cell is optimized with the Hubbard correction applied exclusively on the Ti atom in the cell that is to be reduced. Then, the preoptimized structure will be relaxed again with the Hubbard correction applied on all the Ti atoms. We localize the Ti^{3+} not only in the undercoordinated $Ti(2)O_5$ polyhedron adjacent the O vacancy but also at the next-nearest $Ti(2)O_6$ moiety; also see Fig. 3. These two centers will be denoted as $\mathrm{I}^{\mathrm{O}}_X$ and $\mathrm{II}^{\mathrm{O}}_X$, respectively, whereby O indicates the position of the O vacancy [i.e., either O(9) or O(10)], and X the host material with A = KTP, B = RKTP, C = KTP-K1, and D = KTP-K2. The choice of reducing Ti(2) sites exclusively might appear quite restrictive at first sight, but it is robust for two reasons: First, upon Ti(1) reduction only three ^{31}P nuclei show a relevant hyperfine structure (see also Ref. [35]). Second, as discussed in Refs. [70,71], in KTP isomorphs electrons are trapped in a ferroelectric spin configuration and Ti(2) sites are more prone to reduce compared to Ti(1) sites. At this point, the reader may argue that some of the centers resolved by Setzler *et al.* have been attributed to Ti(1) sites in the cell [34,35]. Nevertheless, since these centers are not thermally stable [34], their presence should not falsify this assumption.

A schematic representation of all $V^{+1}_{\mathrm{O(9)}}$ and $V^{+1}_{\mathrm{O(10)}}$ defect structures after geometry optimization is depicted in Fig. 2. Oxygen vacancies at sites O(9) and O(10) obviously provoke a rather strong geometry relaxation of the surrounding TiO_5 polyhedra. However, the potassium sublattice is also affected to different extents. Notably, in both KTP and RKTP, the vacancy $V^{+1}_{\mathrm{O(10)}}$ causes a stronger disorder compared to $V^{+1}_{\mathrm{O(9)}}$: During geometry relaxation, the K ions are shifted by up to 1.2 Å and less than 0.5 Å, respectively. In K-deficient KTP, in contrast, there is no evident trend, apart from the fact that a $V^{+1}_{\mathrm{O(9)}}$ in KTP-K1 yields the strongest, while a $V^{+1}_{\mathrm{O(10)}}$ in KTP-K1 gives rise to a rather minor rearranging.

We note that in all investigated cases, the strongly localized Ti^{3+} center gives rise to a midgap level in the fundamental band gap, the position of which depends on the

TABLE I. Absolute values of the hyperfine tensors A_1, A_2, and A_3 (in MHz) of all the ^{31}P nuclei showing a relevant hyperfine splitting caused by the O-vacancy related Ti^{3+} centers I_X^O and II_X^O in four different host materials, and the center II_A^K caused by a K interstitial in KTP. The experimental values are taken from Ref. [34]. Note that the experimental tensors are sorted in descending order; the DFT values correspond to their exact attribution.

			KTP					RKTP				KTP-K1				KTP-K2			
		Expt. [34]	$V_{O(9)}^{+1}$		$V_{O(10)}^{+1}$		K_i^0	$V_{O(9)}^{+1}$		$V_{O(10)}^{+1}$		$V_{O(9)}^{+1}$		$V_{O(10)}^{+1}$		$V_{O(9)}^{+1}$		$V_{O(10)}^{+1}$	
Nucleus	tensors	A_{flx}	$I_A^{O(9)}$	$II_A^{O(9)}$	$I_A^{O(10)}$	$II_A^{O(10)}$	II_A^K	$I_B^{O(9)}$	$II_B^{O(9)}$	$I_B^{O(10)}$	$II_B^{O(10)}$	$I_C^{O(9)}$	$II_C^{O(9)}$	$I_C^{O(10)}$	$II_C^{O(10)}$	$I_D^{O(9)}$	$II_D^{O(9)}$	$I_D^{O(10)}$	$II_D^{O(10)}$
	A_1	16.58	31.342	18.850	21.290	19.475	4.0863	32.059	18.903	21.698	18.438	25.394	22.030	23.033	26.348	26.822	21.103	19.980	19.910
^{31}P(1):	A_2	16.75	30.620	18.384	20.831	19.165	2.7694	31.328	18.472	21.245	18.172	24.312	21.623	22.372	25.974	26.151	20.658	18.815	19.762
	A_3	23.36	35.627	24.669	26.161	25.742	7.6468	36.395	24.859	26.588	24.713	32.107	28.222	27.495	33.086	31.180	27.199	27.583	26.368
	A_1	14.28	12.476	12.789	17.692	16.751	2.9712	11.508	12.422	17.307	17.271	19.642	7.867	14.945	13.689	12.937	9.714	15.423	11.303
^{31}P(2):	A_2	14.68	12.048	12.250	17.224	16.510	1.8310	11.066	11.911	16.884	17.046	18.428	7.433	14.474	13.515	12.449	9.252	14.057	11.054
	A_3	21.37	17.592	18.650	23.489	23.104	6.2391	16.529	18.265	23.198	23.725	27.195	13.271	20.273	19.562	18.428	15.258	20.248	16.748
	A_1	3.74	1.585	5.548	2.983	5.493	2.0673	1.063	6.514	3.190	5.581	0.146	7.080	2.372	4.447	1.579	5.342	0.048	7.225
^{31}P(3):	A_2	4.24	0.179	4.489	1.549	4.399	1.0761	0.331	5.453	1.722	4.461	1.364	5.892	0.859	3.231	0.265	4.266	1.357	6.036
	A_3	7.23	3.399	8.357	5.123	8.317	4.6415	2.793	9.449	5.336	8.417	2.141	10.035	4.466	7.173	3.466	8.102	2.128	10.243
	A_1	0.84	0.108	2.806	1.603	1.883	0.4306	0.257	2.964	1.722	2.290	0.815	2.599	1.654	2.526	0.782	1.149	0.631	2.769
^{31}P(4):	A_2	1.40	1.205	1.682	2.760	0.698	0.3987	1.336	1.837	2.865	1.089	0.484	1.340	2.860	1.194	1.819	0.052	0.912	1.512
	A_3	3.94	1.453	5.406	0.168	4.116	2.9198	1.294	5.626	0.292	4.578	2.678	5.219	0.368	4.660	0.777	3.540	2.486	5.404

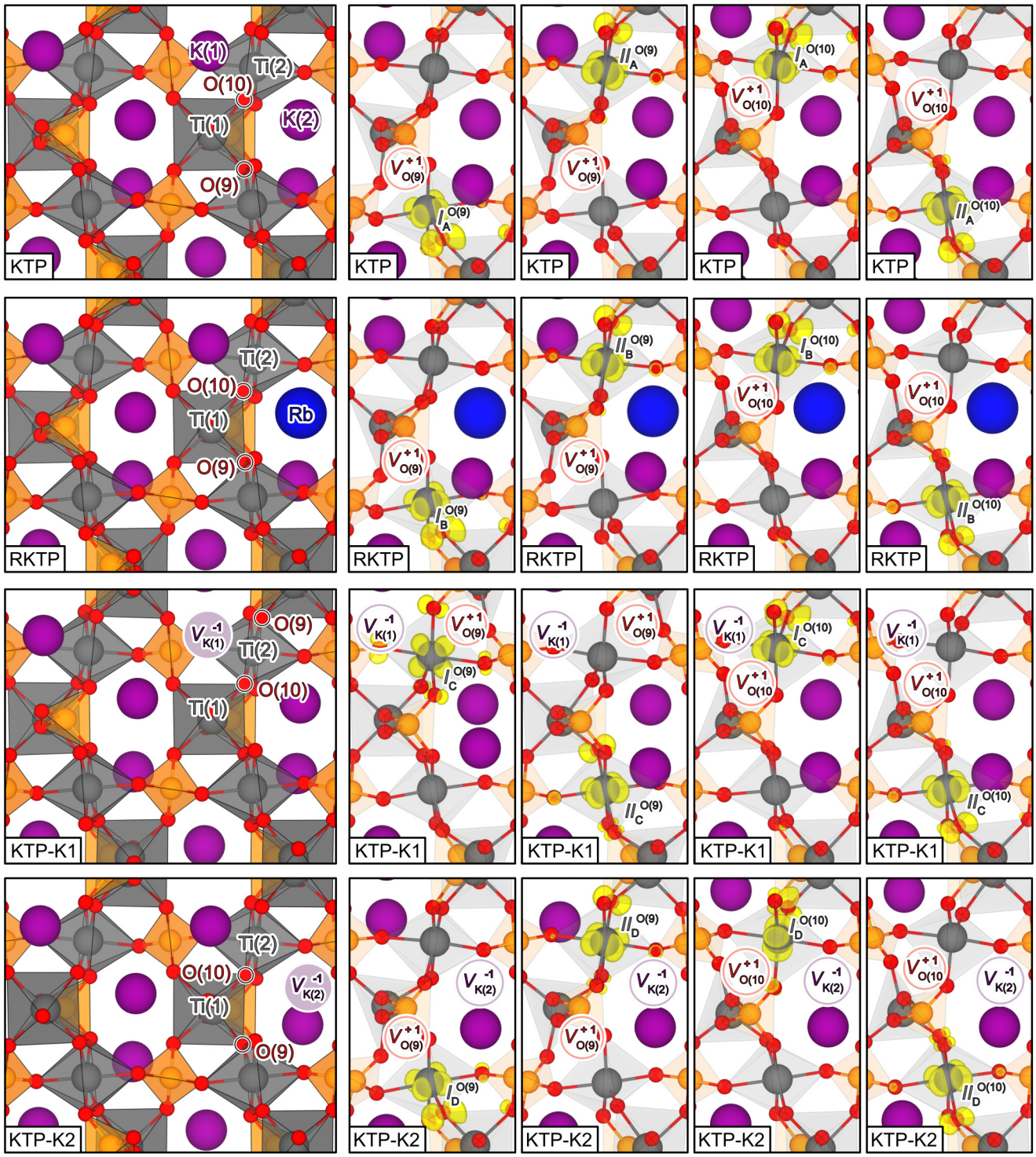

FIG. 2. Schematic representation of the four investigated host materials before and after the introduction of O(9) and O(10) vacancies (for details, see Sec. III). The yellow surfaces correspond to the charge density of the midgap state attributable to the Ti^{3+} centers I^{O}_{X} and II^{O}_{X}. Note that the positions of $I^{O(9)}_{C}$ and $II^{O(9)}_{C}$ differ from the ones assumed in the remaining cells, since the O(9) vacancy is located at a different position. Adapted from Ref. [40].

chosen functional; also see Fig. 4. Although we will refrain from a detailed quantitative analysis of defect-induced absorption at this point, we would like to point out that while the Rb substitutional barely affects the midgap states' position, the K vacancy shifts them slightly toward the conduction band.

IV. HYPERFINE TENSORS

The hyperfine splitting of the resonance lines in electron paramagnetic resonance (EPR) is a consequence of the interaction of the nuclear moments with electron spin. It probes the wave functions of the unpaired electrons at the nuclei and is

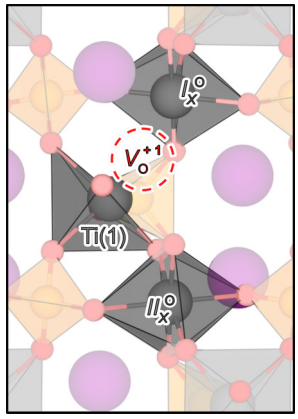

FIG. 3. Relative position of the centers I_X^O and II_X^O and the oxygen vacancy before geometry relaxation: The former is located at an undercoordinated Ti(2)O_5 moiety, the latter at the next-nearest Ti(2)O_6 moiety. Adapted from Ref. [40].

by this extremely sensitive to the chemical environment (see also Sec. II). Thus, these signatures can be used to identify localized states, e.g., defects in crystal structures. Unfortunately, the natural abundance of the EPR-active Ti isotopes

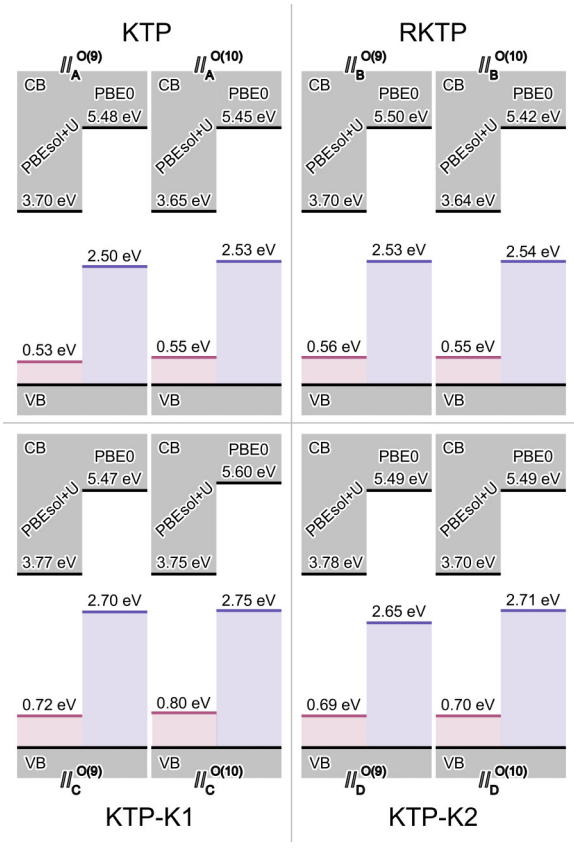

FIG. 4. Position of O-vacancy-related midgap states as determined within the PBEsol + U and the PBE0 formalism caused by the energetically more favorable centers II_X^O. Note that under the application of the PBE0–7% (see main text) their position with respect to the valence band is barely affected compared to the ones obtained using the standard PBE0 functional.

TABLE II. Distances between the Ti^{3+} centers I_X^O and II_X^O and the nearest K^+ ion.

	KTP		RKTP		KTP-K1		KTP-K2	
	$I_A^{O(9)}$	$II_A^{O(9)}$	$I_B^{O(9)}$	$II_B^{O(9)}$	$I_C^{O(9)}$	$II_C^{O(9)}$	$I_D^{O(9)}$	$II_D^{O(9)}$
$\overline{KTi^{3+}}$ [Å]	3.75	3.63	3.75	3.61	3.87	3.55	3.82	3.57
	$I_A^{O(10)}$	$II_A^{O(10)}$	$I_B^{O(10)}$	$II_B^{O(10)}$	$I_C^{O(10)}$	$II_C^{O(10)}$	$I_D^{O(10)}$	$II_D^{O(10)}$
$\overline{KTi^{3+}}$ [Å]	3.87	3.63	3.86	3.63	3.66	3.55	3.88	3.74

(7.4% ^{47}Ti, $I = 5/2$, and 4.4% ^{49}Ti, $I = 7/2$) is not sufficient to allow a resolution of the Ti-related hyperfine signatures in experiment. Also the oxygen isotope with nonzero nuclear spin (^{17}O, $I = 5/2$) has an abundance below 0.04% and is thus far below the resolution limit. For this reason, we have to focus on the hyperfine structure of the surrounding ^{31}P(i) nuclei, see Table I. Note that we only report centers with a relevant hyperfine splitting and they do not necessarily correspond to the same P atoms in different hosts. The comparison of the calculated data with the experimental hyperfine splitting from Ref. [34] for KTP is justified as K vacancies are always present in real KTP crystals [1] and the signatures of Ti^{3+} centers in RTP are very close to the ones in KTP, cf. Refs. [34,41].

For both KTP and RKTP, all the simulated vacancies lead to qualitatively good agreement with experiment. Even O vacancies in K-deficient KTP lead to very similar hyperfine splittings. Notably, the signatures of the centers $II_X^{O(9),\,O(10)}$ [which again are located at the second next-nearest Ti(2) atom] are always in better quantitative agreement with the experiment compared to $I_X^{O(9),\,O(10)}$ located at the undercoordinated TiO_5 moieties. This holds especially for the ^{31}P(3) and ^{31}P(4) nuclei, whereby this behavior is even more pronounced for O vacancies in K-deficient KTP. Thus, the agreement between experimental and theoretical hyperfine tensors is improved for a Ti^{3+} center located at a Ti(2)O_6 moiety close to the O vacancy compared to the previously assigned site. The local chemical environment, on the other hand, does not strongly influence the centers' hyperfine structure.

To better understand these findings, we have to focus on the specific properties of the defects. Notably, the different ^{31}P-related hyperfine splittings caused by the centers I_X^O and II_X^O cannot be explained by different distances between P and Ti. For example, the centers $II_C^{O(10)}$ and $II_D^{O(10)}$ are located at exactly the same position, see Fig. 2, but clearly differ with respect to their hyperfine structure.

As the major difference between the two structures lays in the position the K ions, the hyperfine structure appears to be directly influenced by the K sublattice. In each investigated host material, the center II_X^O is located on average 0.19 Å closer to a K^+ ion compared to the respective I_X^O center; see also Table II. We thus suggest that the K^+ ions provide the stabilizing forces for the trapped electrons and, therefore, for the thermally stable Ti^{3+} center (A_{flx} [23,34]).

By this, our calculations support the finding of previous studies [27,72,73] that K ions may migrate simultaneously

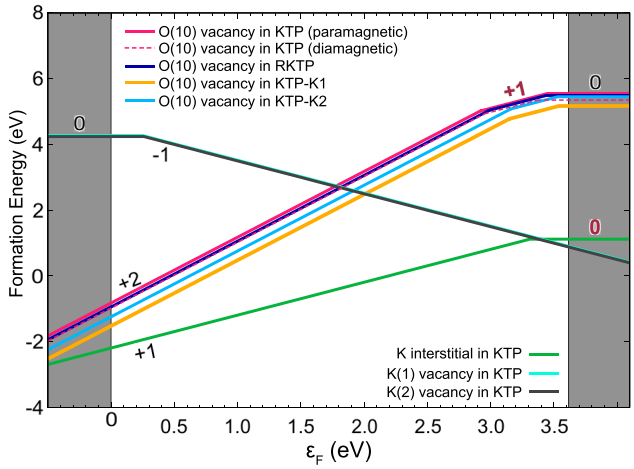

FIG. 5. Formation energy of a O(10) vacancy in four different materials, as well as K interstitial and K vacancies in KTP calculated on the PBE0–7% level of theory. In each case, the formation energy is referred to as the host material. The energy range for the Fermi level ε_F corresponds to the band gap of KTP, the ones of RKTP and KTP-K1 (KTP-K2) do not deviate more than 0.1 eV from this value. The charge states yielding the hyperfine structure discussed in Table I are marked in red.

with their trapped electrons and also play a decisive role in the context of gray tracking. A study by Mürk *et al.* [27] presented gray tracking as characterized by two stages: The first corresponds to (not-further specified) preradiational defects and the second to defects caused by the radiation itself. Thereby, electron-hole pairs stabilized by K interstitials and O atoms are indicated as the origin of the coloring. The authors also found that the transparency of KTP crystals upon the irradiation with x-rays can be preserved by increasing the rigidity of the K sublattice. Mu and Ding [72] attributed the origin of (as they called it) invisible damage to K ions displaced along the [001] crystal direction. Furthermore, Wang *et al.* [73] attributed the increased absorption in periodically poled KTP compared to single-domain crystals to a higher number of K vacancies and interstitials caused by the poling process itself.

Thus, to better understand the microscopic effects accompanying displaced K ions in the context of gray tracking, in the following we extend our investigations onto K interstitials. For this purpose, we model a neutral K interstitial within an otherwise stoichiometric KTP unit cell. Also in this case, the extra electron is localized at the Ti(2) closest to the interstitial. As expected, the hyperfine signatures of this Ti^{3+} center (II_A^K) differ from the signatures of the other centers here simulated, see also Table I, and therefore also from the signatures of the gray-tracking related center reported experimentally [34]. This does not mean, however, that K interstitials have to be excluded completely. Due to the position of the $(+1/0)$ charge transition very close to the CBM (see Fig. 5), the K interstitials are expected to be in their diamagnetic, i.e., EPR-silent charge state in most cases. Hence, in the following, we will discuss the energetics and absorption properties of the O vacancies as well as the K interstitial.

TABLE III. Differences of the PBE0 ground-state energy of the centers I_X^O and II_X^O caused by the same O vacancy in each host material X.

Host	KTP (A)		RKTP (B)		KTP-K1 (C)		KTP-K2 (D)	
O vacancy	$V_{O(9)}^{+1}$	$V_{O(10)}^{+1}$	$V_{O(9)}^{+1}$	$V_{O(10)}^{+1}$	$V_{O(9)}^{+1}$	$V_{O(10)}^{+1}$	$V_{O(9)}^{+1}$	$V_{O(10)}^{+1}$
ΔE [meV]	+241	+164	+223	+166	+291	+146	+247	+188

V. ENERGETICS

To determine the relative stability of the centers $I_X^{O(9),O(10)}$ and $II^{O(9),O(10)}$ in each material X, we analyze the energy difference

$$\Delta E = E_{\mathrm{I}} - E_{\mathrm{II}}, \tag{5}$$

where E_{I} and E_{II} correspond to the PBE0 ground-state energy of the material X containing the centers $I_X^{O(9),O(10)}$ and $II_X^{O(9),O(10)}$, respectively. The so-calculated values are compiled in Table III. All the energy differences are positive (between +146 meV and +291 meV), meaning that the cells containing the center $II_X^{O(9),O(10)}$ are always energetically more favorable than the scenario, where the Ti^{3+} center is localized adjacent the O vacancy, i.e., the center $I_X^{O(9),O(10)}$.

In the second step, we compute the formation energy of charged oxygen vacancies as a function of the Fermi-level position ε_F via Eqs. (1) and (2). Since the vacancies O(9) and O(10) are expected to show the same qualitative trends, we limit our detailed discussions to the O(10) vacancy. In addition, the ground-state energies and chemical potentials as well as energetic position of half-occupied levels are determined using the PBE0–7% functional (i.e., a modification of the PBE0 functional including 7% of EXX; see also next section), since this yields agood agreement with the experimental KTP band gap, so the energetic position of the states are expected to be reliable. In fact, as discussed previously [38], the energetic position of the occupied midgap defect state measured from the VBM does not change significantly compared to its position under the application of the standard PBE0 functional. The formation energy of the O(10) vacancy in four different hosts is depicted in Fig. 5. Here, we also show the formation energy of a K interstitial in KTP and the one of the K(1) and K(2) vacancies in KTP. Note that in each case the energy is referred to the ground-state energy of the host material, which in the case of a O vacancy in K-deficient KTP is negatively charged. In addition, the indicated Fermi-level range refers to the band gap of bulk KTP. The ones of RKTP, KTP-K1, and KTP-K2 deviate not more than 0.1 eV from this value. Due to the choice of referring the formation energy to the host materials, the O vacancy can assume three different charge states: Within the charge state +2, there is no trapped defect electron and the related defect states are completely emptied. For charge state +1, we choose the cell where the trapped electron yields the more favorable center $II_X^{O(10)}$. For the neutral, on the other hand, there are many possibilities. Two reasonable choices are (i) in a diamagnetic spin configuration $S = 0$, with the electrons localized at the center $II_X^{O(10)}$ and at the $Ti(1)O_5$ moiety caused by the O vacancy, and (ii) a spin-triplet $S = 1$ configuration, where the electrons are

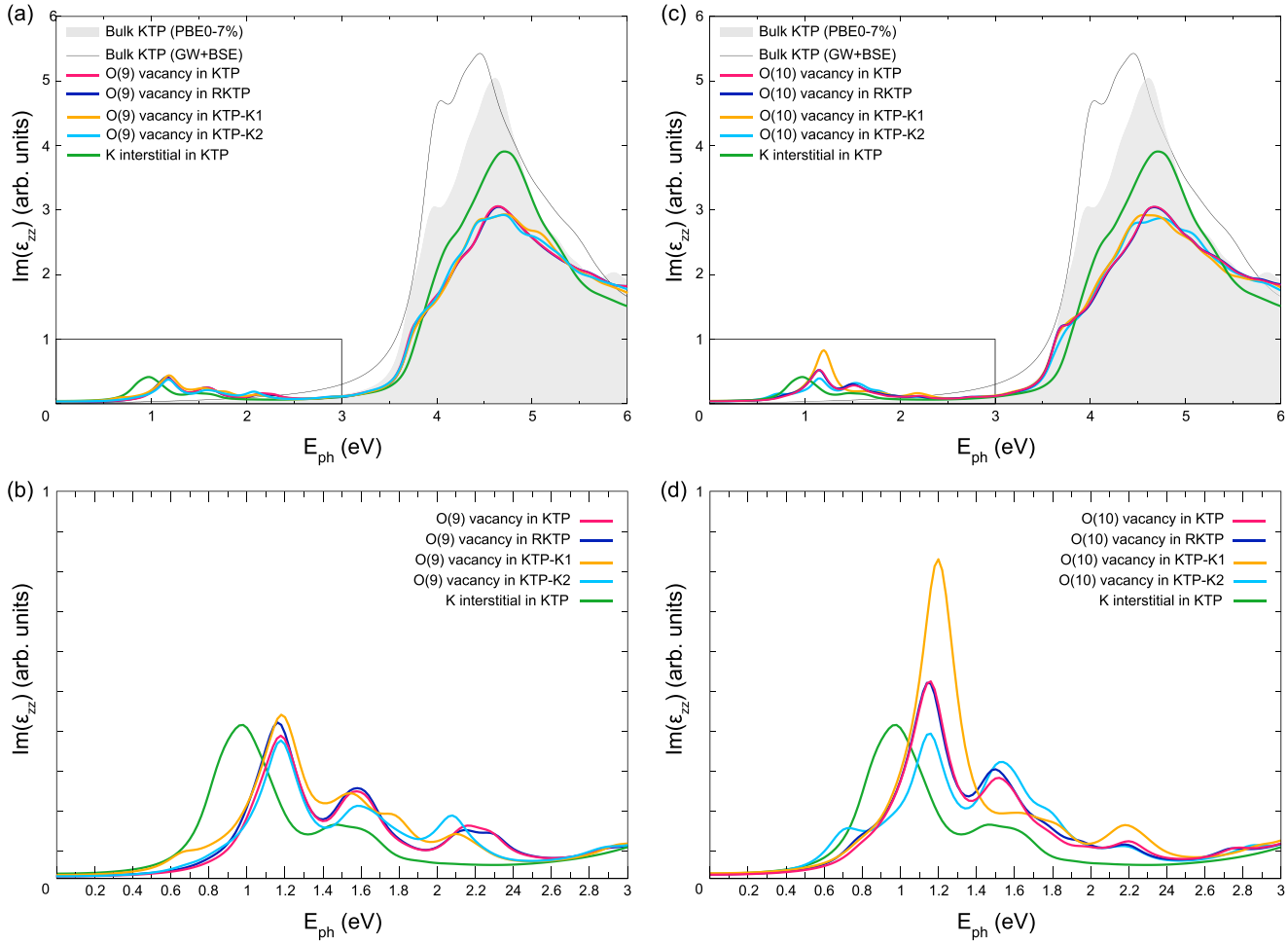

FIG. 6. (a), (c) Imaginary parts of the dielectric function as a function of the photon energy E_{ph} calculated using the PBE0–7% method (for further details, see text) of the centers II_X^{O} in different materials caused by the vacancies O(9) and O(10), respectively. The filled gray curve refers to bulk KTP, while the GW + BSE spectrum (black line) is taken from Ref. [53]. (b), (d) Enlarged representations of the insets marked in (a) and (b), respectively. Note that only the z component, i.e., Im(ε_{zz}), most relevant for gray tracking [18–20,29] is shown.

trapped at both the $\mathrm{I}_X^{\mathrm{O}(10)}$ and $\mathrm{II}_X^{\mathrm{O}(10)}$ centers in a paramagnetic spin configuration. We find that they provide almost the same formation energy profile, cf. solid and dashed magenta curves in Fig. 5. So, due to the similarity of the results and and the particular reduction sequence of Ti sites in KTP isomorphs [70,71], only the latter configuration will be taken into account for the remaining systems.

The formation energy of the O vacancy does not strongly depend on the host material: In every investigated case, the charge state +2 is the dominating one for a broad range of Fermi-level positions, while the EPR-active charge state +1 is only stable for a narrow energy range close to the conduction band. However, in contrast to what was found in Ref. [35] within PBEsol + U, the formation of neutral vacancies seems to be excluded, at least for moderately n-type doped material. For the K interstitial and vacancy, the dominant state is the single positively and the single negatively charged ones, respectively. The formation energy of the interstitial is notable lower compared to the one of the O vacancies in different materials so its formation is in fact not to be excluded. Furthermore, we find that in the presence of a K vacancy, the O vacancy is more prone to form close to this vacancy, while the K_i^+ is not likely to form, meaning that K-Frenkel pairs are rather unlikely in this class of material.

VI. OPTICAL ABSORPTION

In the previous section (cf. Fig. 5), we have shown that the vacancy PBE0–7% formation energy renders the neutral charge state unstable or at least very unlikely. This finding somewhat questions the hypothesis that the different stages of gray tracking could be related to different charge states assumed by the O vacancy itself [38]. To investigate the influence of the chemical environment onto the optical properties, we calculate the optical absorption spectra of the gray-tracking relevant $\mathrm{II}_X^{\mathrm{O}}$ centers and the Ti^{3+} center caused by the K interstitial $\mathrm{II}_A^{\mathrm{K}}$ by adopting a modification of the method discussed in Ref. [38].

Due to the use of a different Ti pseudopotential, the fraction of EXX required to reproduce the GW + BSE gap [53] has to be lowered from 10% to 7% (i.e., PBE0–7%). The imaginary parts of the z component of the resulting dielectric function ε_{zz}

are shown in Fig. 6. The PBE0–7% method provides a good approximation of a previous *GW* + BSE study [53], which also includes excitonic quasiparticle effects. The inserted defects provoke a redistribution of the oscillator strengths: The intensity of the main absorption peak is lowered, simultaneously new absorption signatures caused by the excitation of the defect-related midgap states appear for below-gap photon energies; see Fig. 6(b). More precisely, we find that the absorption properties of O-vacancy related Ti^{3+} centers are not influenced by Rb dopants, cf. pink and dark blue curves in Fig. 6. Both in fact show basically the same line shape with absorption maxima at about 1.1–1.2 eV (main defect peak), 1.5–1.6 eV and 2.1–2.3 eV. More precisely, in the case of the O(9) vacancies the main peak is slightly blueshifted to about 1.2 eV and reduced in intensity, while the one at around 2.2 eV results to be broader and higher in intensity compared to the ones of O(10) vacancies.

In K-deficient KTP, the exact location of the K vacancy has a strong influence on the spectral shape: The main impact is found for the O(10) vacancy in KTP-K1, where the intensity of the main peak is blueshifted to about 1.2 eV, and also the intensity of the peak at about 2.2 eV is enhanced. For the O(10) vacancy in KTP-K2, in contrast, the shoulders on the left and the right sides of the spectrum become more pronounced. O(9) vacancies, on the other hand, show qualitatively the same trends in both materials: The main effect is a slight redshift of the third absorption peak to a photon energy of about 2.1 eV. Interestingly, the absorption properties of the K interstitial are also close to the ones of O vacancies with broad absorption peaks centered at about 1.0 eV and in the range of about 1.4–1.7 eV, but with missing peak at 2.2 eV.

VII. DISCUSSION

The results presented in the last sections show that the currently accepted gray-tracking model has to be partially revised. First, our data clearly show that Ti^{3+} centers localized at undercoordinated $Ti(2)O_5$ moieties caused by a O vacancy itself are not only energetically less stable compared to Ti^{3+} centers located at a $Ti(2)O_6$ moiety close to the O vacancy. Also, the agreement with experimental hyperfine tensors [34] is quantitatively improved in the latter case. Thereby, displaced K ions are shown to provide the required stabilizing forces.

The data also indicate that the attribution of different stages of gray tracking to a gradual charging of the oxygen vacancy [38] does not provide a fully satisfactory explanation for the phenomenon, since the neutral charge state is not predicted to be sufficiently stable. Nevertheless, we still expect O vacancies to play a decisive role in the formation of the Ti^{3+} centers: The vacancy, in fact, causes the displacement of the K sublattice, which then provides the stabilizing (electrostatic) forces for the Ti^{3+} centers.

In addition, the formation energy of the O vacancy in different materials shows that the EPR-active charge state related to gray tracking is only stable for high positions of the Fermi level, i.e., for strongly *n*-type doped material, which is clearly given in the case of K-deficient KTP. For stoichiometric as well as Rb-doped KTP, on the other hand, only the charge state +2, not showing any occupied midgap states and related absorption signatures (see Ref. [38]) appears to be sufficiently stable.

The finding that the presence of K vacancies is crucial for gray tracking is further reinforced by the fact that the absorption characteristics of the O vacancy in K-deficient KTP can be directly related to the first- and the second-harmonic radiation at 1064 nm and 532 nm [17–20,25,29] (i.e., about 1.17 eV and 2.33 eV), respectively, corresponding to the absorption characteristics of gray tracks. The absorption signatures of O vacancies in stoichiometric and Rb-doped KTP, on the other hand, may only approximate the 1064 nm radiation. Interestingly the absorption characteristics of a neutral K interstitial also fall in the same energy range. However, the method presented in Ref. [38] and adopted here for the calculation of the vacancies' absorption properties highly benefits from error cancellation and may not account correctly for many-body effects for all configurations considered. Verified using *GW* + BSE studies [53,68] for stoichiometric KTP, it might not provide a perfect description of all defect-related effects, so the participation of K interstitials cannot be excluded. This possibility is in line with the observation that the loss of K [74,75] and P [75], which determines the thermal decomposition of KTP surfaces, results in a translucent layer, whereby its removal during cooling restores the crystal transparency [75].

Furthermore, our investigation suggests the possibility of a simultaneous migration of K interstitials and their trapped electron through the crystal upon the application of electric fields or the irradiation with laser light. The formation of overpopulated K-migration channels could explain both the shape of gray tracks induced by the application of high-voltage pulses along the *c* axis (i.e., dark needles originating at one electrode and growing in direction of the other) [26] and also the reduced ionic conductivity of gray-tracked areas [26], since they would naturally contrast vacancy hopping mechanisms. In addition, the K-interstitial model could also provide an explanation why Rb dopants are beneficial for their suppression: (i) Rb dopants, by means of reducing the number of K vacancies, not only contrast the formation of the detrimental charge state +1 but (ii) they could also prevent overpopulated K channels, since they are characterized by a higher activation energy for migration [26].

VIII. SUMMARY

Our comprehensive and systematic investigation of O vacancies within stoichiometric, K-deficient, and Rb-doped KTP let us refine and partially revise the defect model attributed to the so-called gray tracking of the material.

First, our data suggest that the position of the Ti^{3+} has to be shifted from the adjacent $Ti(2)O_5$ to the next-nearest $Ti(2)O_6$ moiety, considering that the latter scenario (i.e., the II_X^O center) does not only yield better agreement with experimental hyperfine structure but is also energetically more favorable.

In addition, although O-vacancy-related Ti^{3+} centers are usually considered as the microscopic origin of macroscopic gray tracks, our results suggest that O vacancies alone are not able to explain all the details of gray tracking sufficiently well. We rather suggest that gray tracking should be attributed to a

vacancy pair composed of a positively charged O vacancy and a negatively charged K vacancy. However, also, in this context displaced K ions leading to the formation of overpopulated K channels cannot be completely excluded as a possible explanation for gray-track formation.

We expect that our paper will be instrumental in fully clarifying the gray-track formation mechanisms and paves the way to further experimental and theoretical investigation. In particular, the investigation of the interplay between O-vacancy related Ti^{3+} centers and K vacancies, displaced K ions as well as K interstitials, and most importantly their simultaneous migration through the crystal, is highly desirable.

ACKNOWLEDGMENTS

The authors gratefully acknowledge financial support from DFG (TRR 142/3-2025—Project No. 231447078), and computational resources provided by the Paderborn Center for Parallel Computing (PC^2), and the High Performance Computing Center Stuttgart (HLRS).

[1] M. Roth, Stoichiometry and domain structure of KTP-type nonlinear optical crystals, in *Springer Handbook of Crystal Growth*, edited by G. Dhanaraj, K. Byrappa, V. Prasad, and M. Dudley (Springer, Berlin, 2010), Chap. 20, pp. 691–723, and references within.

[2] N. I. Sorokina and V. I. Voronkova, Structure and properties of crystals in the potassium titanyl phosphate family: A review, Crystallogr. Rep. **52**, 80 (2007).

[3] J. E. Lowther, P. Manyum, and P. Suebka, Electronic and structural properties of orthorhombic $KTiOPO_4$ and related isomorphic materials, Physica Status Solidi (b) **242**, 1392 (2005).

[4] J. D. Bierlein and H. Vanherzeele, Potassium titanyl phosphate: Properties and new applications, J. Opt. Soc. Am. B **6**, 622 (1989).

[5] F. C. Zumsteg, J. D. Bierlein, and T. E. Gier, $K_xRb_{1-x}TiOPO_4$: A new nonlinear optical material, J. Appl. Phys. **47**, 4980 (1976).

[6] G. Qiu, H. T. Huang, B. T. Zhang, J. L. He, J. F. Yang, and J. L. Xu, Highly efficient intracavity frequency doubling 532-nm laser based on the gray tracking resistance KTP crystal, Laser Phys. **20**, 777 (2010).

[7] A. H. Reshak, I. V. Kityk, and S. Auluck, Investigation of the linear and nonlinear optical susceptibilities of $KTiOPO_4$ single crystals: Theory and experiment, J. Phys. Chem. B **114**, 16705 (2010).

[8] I. Savatinova, I. Savova, E. Liarokapis, C. C. Ziling, V. V. Atuchin, M. N. Armenise, and V. M. N. Passaro, A comparative analysis of Rb:KTP and Cs:KTP optical waveguides, J. Phys. D **31**, 1667 (1998).

[9] M. Peltz, U. Bäder, A. Borsutzky, R. Wallenstein, J. Hellström, H. Karlsson, V. Pasiskevicius, and F. Laurell, Optical parametric oscillators for high pulse energy and high average power operation based on large aperture periodically poled KTP and RTA, Appl. Phys. B **73**, 663 (2001).

[10] M. N. Satyanarayan, A. Deepthy, and H. L. Bhat, Potassium titanyl phosphate and its isomorphs: Growth, properties, and applications, Crit. Rev. Solid State Mater. Sci. **24**, 103 (1999).

[11] C. Eigner, L. Padberg, M. Santandrea, H. Herrmann, B. Brecht, and C. Silberhorn, Spatially single mode photon pair source at 800 nm in periodically poled rubidium exchanged KTP waveguides, Opt. Express **28**, 32925 (2020).

[12] J. D. Bierlein and C. B. Arweiler, Electro-optic and dielectric properties of $KTiOPO_4$, Appl. Phys. Lett. **49**, 917 (1986).

[13] X. D. Wang, P. Basseras, R. J. D. Miller, and H. Vanherzeele, Investigation of $KTiOPO_4$ as an electro-optic amplitude modulator, Appl. Phys. Lett. **59**, 519 (1991).

[14] M. Roth, N. Angert, M. Tseitlin, and A. Alexandrovski, On the optical quality of KTP crystals for nonlinear optical and electro-optic applications, Opt. Mater. (Amsterdam) **16**, 131 (2001).

[15] L. Mu, L. Ben, Y.-S. Hu, H. Li, L. Chen, and X. Huang, Novel 1.5 V anode materials, $ATiOPO_4$ (A = NH_4, K, Na), for room-temperature sodium-ion batteries, J. Mater. Chem. A **4**, 7141 (2016).

[16] S. Liu, L. Shao, X. Zhang, M. Zhou, Z. Tao, and J. Chen, $KTiOPO_4$ as a novel anode material for sodium-ion batteries, J. Alloys Compd. **754**, 147 (2018).

[17] B. Boulanger, M. M. Fejer, R. Blachman, and P. F. Bordui, Study of $KTiOPO_4$ gray-tracking at 1064, 532, and 355 nm, Appl. Phys. Lett. **65**, 2401 (1994).

[18] B. Boulanger, I. Rousseau, J. P. Fève, M. Maglione, B. Menaert, and G. Marnier, Optical studies of laser-induced gray-tracking in KTP, IEEE J. Quantum Electron. **35**, 281 (1999).

[19] V. A. Maslov, V. A. Mikhailov, O. P. Shaunin, and I. A. Shcherbakov, Nonlinear absorption in KTP crystals, Quantum Electron. **27**, 356 (1997).

[20] G. M. Loiacono, D. N. Loiacono, T. McGee, and M. Babb, Laser damage formation in $KTiOPO_4$ and $KTiOAsO_4$ crystals: Grey tracks, J. Appl. Phys. **72**, 2705 (1992).

[21] N. B. Angert, V. M. Garmash, N. I. Pavlova, and A. V. Tarasov, Influence of color centers on the optical properties of KTP crystals and on the efficiency of the laser radiation frequency conversion in these crystals, Sov. J. Quantum Electron. **21**, 426 (1991).

[22] L. E. Halliburton and M. P. Scripsick, Mechanisms and point defects responsible for the formation of gray tracks in KTP, in *Proceedings of the Solid State Lasers and Nonlinear Crystals* (SPIE, 1995), Vol. 2379, pp. 235–244.

[23] M. G. Roelofs, Identification of Ti^{3+} in potassium titanyl phosphate and its possible role in laser damage, J. Appl. Phys. **65**, 4976 (1989).

[24] F. R. Wagner, G. Duchateau, J.-Y. Natoli, H. Akhouayri, and M. Commandré, Catastrophic nanosecond laser induced damage in the bulk of potassium titanyl phosphate crystals, J. Appl. Phys. **115**, 243102 (2014).

[25] A. Alexandrovski, M. Fejer, and G. Mitchell, CW gray-track formation in KTP, in *Technical Digest. Summaries of papers presented at the Conference on Lasers and Electro-Optics. Postconference Edition. CLEO '99. Conference on Lasers and Electro-Optics (IEEE Cat. No. 99CH37013)* (IEEE, Piscataway, NJ, 1999), pp. 531–532.

[26] L. Padberg, V. Quiring, A. Bocchini, M. Santandrea, U. Gerstmann, W. G. Schmidt, C. Silberhorn, and C. Eigner, DC

ionic conductivity in KTP and its isomorphs: Properties, methods for suppression, and its connection to gray tracking Crystals **12**, 1359 (2022).

[27] V. Mürk, V. Denks, A. Dudelzak, P.-P. Proulx, and V. Vassiltsenko, Gray tracks in $KTiOPO_4$: Mechanism of creation and bleaching, Nucl. Instrum. Methods Phys. Res., Sect. B **141**, 472 (1998).

[28] Y. Zhang, H. Wang, C. Ma, Y. Jia, J. Li, J. Wang, R. Boughton, and H. Jiang, Growth and optical properties of gray-track-resistant $KTiOPO_4$ single crystals, J. Cryst. Growth **412**, 67 (2015).

[29] B. V. Andreev, V. A. Maslov, B. A. Mikhailov, S. K. Pak, O. P. Shaunin, and I. A. Shcherbakov, Experimental study of the laser-induced absorption effect and the nature of color centers in potassium titanyl phosphate crystal, in *Proceedings of the Solid State Lasers and New Laser Materials*, edited by Vyacheslav V. Osiko, International Society for Optics and Photonics (SPIE, 1992), Vol. 1839, pp. 280–289.

[30] Q. Zhang, G. Feng, J. Han, B. Li, Q. Zhu, and X. Xie, High repetition rate laser pulse induced damage in KTP crystal: Gray-tracking and catastrophic damage, Optik **122**, 1313 (2011).

[31] M. P. Scripsick, G. J. Edwards, L. E. Halliburton, R. F. Belt, and G. M. Loiacono, Effect of crystal growth on Ti^{3+} centers in $KTiOPO_4$, J. Appl. Phys. **76**, 773 (1994).

[32] G. J. Edwards, M. P. Scripsick, L. E. Halliburton, and R. F. Belt, Identification of a radiation-induced hole center in $KTiOPO_4$, Phys. Rev. B **48**, 6884 (1993).

[33] Y. Zhang, Y. Leng, J. Liu, N. Ji, X. Duan, J. Li, X. Zhao, J. Wang, and H. Jiang, Mechanism of hydrogen treatment in $KTiOPO_4$ crystals at high temperature: Experimental and first-principles studies, CrystEngComm **17**, 3793 (2015).

[34] S. D. Setzler, K. T. Stevens, N. C. Fernelius, M. P. Scripsick, G. J. Edwards, and L. E. Halliburton, Electron paramagnetic resonance and electro-nuclear double-resonance study of Ti^{3+} centres in $KTiOPO_4$, J. Phys.: Condens. Matter **15**, 3969 (2003).

[35] A. Bocchini, C. Eigner, C. Silberhorn, W. G. Schmidt, and U. Gerstmann, Understanding gray track formation in KTP: Ti^{3+} centers studied from first principles, Phys. Rev. Mater. **4**, 124402 (2020).

[36] M. P. Scripsick, D. N. Loiacono, J. Rottenberg, S. H. Goellner, L. E. Halliburton, and F. K. Hopkins, Defects responsible for gray tracks in flux-grown $KTiOPO_4$, Appl. Phys. Lett. **66**, 3428 (1995).

[37] A. Bocchini, S. Neufeld, U. Gerstmann, and W. G. Schmidt, Oxygen and potassium vacancies in KTP calculated from first principles, J. Phys.: Condens. Matter **31**, 385401 (2019).

[38] A. Bocchini, U. Gerstmann, and W. G. Schmidt, Oxygen vacancies in $KTiOPO_4$: Optical absorption from hybrid DFT, Phys. Rev. B **105**, 205118 (2022).

[39] A. Zukauskas, V. Pasiskevicius, and C. Canalias, Second-harmonic generation in periodically poled bulk Rb-doped $KTiOPO_4$ below 400 nm at high peak-intensities, Opt. Express **21**, 1395 (2013).

[40] A. Bocchini, Optical and electrochemical properties of KTP-type crystals, Ph.D. thesis, Universität Paderborn, 2023.

[41] Y. Jiang, L. E. Halliburton, M. Roth, M. Tseitlin, and N. Angert, EPR and ENDOR study of an oxygen-vacancy-associated Ti^{3+} center in $RbTiOPO_4$ crystals, Phys. B: Condens. Matter **400**, 190 (2007).

[42] A. Hildenbrand, F. R. Wagner, H. Akhouayri, J.-Y. Natoli, M. Commandré, F. Théodore, and H. Albrecht, Laser-induced damage investigation at 1064 nm in $KTiOPO_4$ crystals and its analogy with $RbTiOPO_4$, Appl. Opt. **48**, 4263 (2009).

[43] A. R. Albuquerque, A. Bruix, I. M. G. dos Santos, J. R. Sambrano, and F. Illas, DFT study on Ce-doped anatase TiO_2: Nature of Ce^{3+} and Ti^{3+} centers triggered by oxygen vacancy formation, J. Phys. Chem. C **118**, 9677 (2014).

[44] K. Momma and F. Izumi, *VESTA3* for three-dimensional visualization of crystal, volumetric and morphology data, J. Appl. Crystallogr. **44**, 1272 (2011).

[45] P. Giannozzi, S. Baroni, N. Bonini, M. Calandra, R. Car, C. Cavazzoni, D. Ceresoli, G. L. Chiarotti, M. Cococcioni, I. Dabo, A. D. Corso, S. de Gironcoli, S. Fabris, G. Fratesi, R. Gebauer, U. Gerstmann, C. Gougoussis, A. Kokalj, M. Lazzeri, L. Martin-Samos, N. Marzari, F. Mauri, R. Mazzarello, S. Paolini, A. Pasquarello, L. Paulatto, C. Sbraccia, S. Scandolo, G. Sclauzero, A. P Seitsonen, A. Smogunov, P. Umari, and R. M. Wentzcovitch, Quantum ESPRESSO: A modular and open-source software project for quantum simulations of materials, J. Phys.: Condens. Matter **21**, 395502 (2009).

[46] P. Giannozzi, O. Andreussi, T. Brumme, O. Bunau, M. B. Nardelli, M. Calandra, R. Car, C. Cavazzoni, D. Ceresoli, M. Cococcioni, N. Colonna, I. Carnimeo, A. D. Corso, S. de Gironcoli, P. Delugas, R. A. DiStasio, A. Ferretti, A. Floris, G. Fratesi, G. Fugallo, R. Gebauer, U. Gerstmann, F. Giustino, T. Gorni, J. Jia, M. Kawamura, H.-Y. Ko, A. Kokalj, E. Küçükbenli, M. Lazzeri, M. Marsili, N. Marzari, F. Mauri, N. L. Nguyen, H.-V. Nguyen, A. O. de-la Roza, L. Paulatto, S. Poncé, D. Rocca, R. Sabatini, B. Santra, M. Schlipf, A. P. Seitsonen, A. Smogunov, I. Timrov, T. Thonhauser, P. Umari, N. Vast, X. Wu, and S. Baroni, Advanced capabilities for materials modelling with Quantum ESPRESSO, J. Phys.: Condens. Matter **29**, 465901 (2017).

[47] A. Marini, C. Hogan, M. Grüning, and D. Varsano, Yambo: An *ab initio* tool for excited state calculations, Comput. Phys. Commun. **180**, 1392 (2009).

[48] D. Sangalli, A. Ferretti, H. Miranda, C. Attaccalite, I. Marri, E. Cannuccia, P. Melo, M. Marsili, F. Paleari, A. Marrazzo, G. Prandini, P. Bonfà, M. O. Atambo, F. Affinito, M. Palummo, A. Molina-Sánchez, C. Hogan, M. Grüning, and D. Varsano, Many-body perturbation theory calculations using the Yambo code, J. Phys.: Condens. Matter **31**, 325902 (2019).

[49] A. Baldereschi, Mean-value point in the Brillouin zone, Phys. Rev. B **7**, 5212 (1973).

[50] P. I. Tordjman, E. Masse, and J. C. Guitel, Crystal structure of monophosphate $KTiPO_5$, Z. Kristal. **139**, 103 (1974).

[51] J. P. Perdew, A. Ruzsinszky, G. I. Csonka, O. A. Vydrov, G. E. Scuseria, L. A. Constantin, X. Zhou, and K. Burke, Restoring the density-gradient expansion for exchange in solids and surfaces, Phys. Rev. Lett. **100**, 136406 (2008).

[52] J. P. Perdew, A. Ruzsinszky, G. I. Csonka, O. A. Vydrov, G. E. Scuseria, L. A. Constantin, X. Zhou, and K. Burke, Erratum: Restoring the density-gradient expansion for exchange in solids

and surfaces [Phys. Rev. Lett. 100, 136406 (2008)], Phys. Rev. Lett. **102**, 039902(E) (2009).

[53] S. Neufeld, A. Bocchini, U. Gerstmann, A. Schindlmayr, and W. G. Schmidt, Potassium titanyl phosphate (KTP) quasiparticle energies and optical response, J. Phys.: Mater. **2**, 045003 (2019).

[54] M. Cococcioni and S. de Gironcoli, Linear response approach to the calculation of the effective interaction parameters in the LDA + U method, Phys. Rev. B **71**, 035105 (2005).

[55] H. P. Li, C. H. Kam, Y. L. Lam, and W. Ji, Femtosecond Z-scan measurements of nonlinear refraction in nonlinear optical crystals, Opt. Mater. (Amsterdam) **15**, 237 (2001).

[56] M. Sheik-Bahae, D. C. Hutchings, D. J. Hagan, and E. W. Van Stryland, Dispersion of bound electron nonlinear refraction in solids, IEEE J. Quantum Electron. **27**, 1296 (1991).

[57] A. Dudelzak, P.-P. Proulx, V. Denks, V. Mürk, and V. Nagirnyi, Anisotropic fundamental absorption edge of $KTiOPO_4$ crystals, J. Appl. Phys. **87**, 2110 (2000).

[58] J. P. Perdew, M. Ernzerhof, and K. Burke, Rationale for mixing exact exchange with density functional approximations, J. Chem. Phys. **105**, 9982 (1996).

[59] P. Deák, M. Lorke, B. Aradi, and T. Frauenheim, Optimized hybrid functionals for defect calculations in semiconductors, J. Appl. Phys. **126**, 130901 (2019).

[60] A. Janotti, J. B. Varley, P. Rinke, N. Umezawa, G. Kresse, and C. G. Van de Walle, Hybrid functional studies of the oxygen vacancy in TiO_2, Phys. Rev. B **81**, 085212 (2010).

[61] H.-P. Komsa, P. Broqvist, and A. Pasquarello, Alignment of defect levels and band edges through hybrid functionals: Effect of screening in the exchange term, Phys. Rev. B **81**, 205118 (2010).

[62] J. C. Slater, Note on Hartree's method, Phys. Rev. **35**, 210 (1930).

[63] J. F. Janak, Proof that $\frac{\partial e}{\partial n_i} = \epsilon$ in density-functional theory, Phys. Rev. B **18**, 7165 (1978).

[64] S. Sanna, Th. Frauenheim, and U. Gerstmann, Validity of the Slater-Janak transition-state model within the LDA+U approach, Phys. Rev. B **78**, 085201 (2008).

[65] C. J. Pickard and F. Mauri, First-principles theory of the EPR g tensor in solids: Defects in quartz, Phys. Rev. Lett. **88**, 086403 (2002).

[66] U. Gerstmann, *Ab initio* Green's function calculation of hyperfine interactions for shallow defects in semiconductors, Phys. Status Solidi B **248**, 1319 (2011).

[67] K. L. Franzke, W. G. Schmidt, and U. Gerstmann, Relativistic calculation of the orbital hyperfine splitting in complex microscopic structures, J. Phys.: Conf. Ser. **2701**, 012094 (2024).

[68] M. Ghoohestani, S. J. Hashemifar, and A. Arab, Linear and nonlinear optical properties of $RbTiOPO_4$–$KTiOPO_4$ alloys studied from first principles, J. Appl. Phys. **128**, 125707 (2020).

[69] P. A. Thomas, R. Duhlev, and S. J. Teat, A comparative structural study of a flux-grown crystal of $K_{0.86}Rb_{0.14}TiOPO_4$ and an ion-exchanged crystal of $K_{0.84}Rb_{0.16}TiOPO_4$, Acta Crystallogr. Sect. B **50**, 538 (1994).

[70] S. S. Fedotov, N. D. Luchinin, D. A. Aksyonov, A. V. Morozov, S. V. Ryazantsev, M. Gaboardi, J. R. Plaisier, K. J. Stevenson, A. M. Abakumov, and E. V. Antipov, Titanium-based potassium-ion battery positive electrode with extraordinarily high redox potential, Nat. Commun. **11**, 1484 (2020).

[71] A. Bocchini, Y. Xie, W. G. Schmidt, and U. Gerstmann, Structural and electrochemical properties of F-doped $RbTiOPO_4$ (RTP:F) predicted from first principles, Crystals **14**, 5 (2023).

[72] X. Mu and Y. J. Ding, Investigation of damage mechanisms of $KTiOPO_4$ crystals by use of a continuous-wave argon laser, Appl. Opt. **39**, 3099 (2000).

[73] S. Wang, V. Pasiskevicius, and F. Laurell, Dynamics of green light-induced infrared absorption in $KTiOPO_4$ and periodically poled $KTiOPO_4$, J. Appl. Phys. **96**, 2023 (2004).

[74] N. Angert, M. Tseitlin, E. Yashchin, and M. Roth, Ferroelectric phase transition temperatures of $KTiOPO_4$ crystals grown from self-fluxes, Appl. Phys. Lett. **67**, 1941 (1995).

[75] M. J. Martín, D. Bravo, R. Solé, F. Díaz, F. J. López, and C. Zaldo, Thermal reduction of $KTiOPO_4$ single crystals, J. Appl. Phys. **76**, 7510 (1994).